Energy-resolved X-ray radiography with Controlled-Drift Detectors at Sincrotrone Trieste

A. Castoldi [a*], A. Galimberti[a], C.Guazzoni [a], P. Rehak [b], L.Strüder [c], R.H. Menk[d]

[a] *Politecnico di Milano, Piazza Leonardo da Vinci 32, 20133 Milano, Italy and INFN Sezione di Milano*

[b]*Brookhaven National Laboratory, Upton, 11973 NY, USA*

[c]*Halbleiterlabor of the Max Planck Institut, Otto-Hahn-Ring 6, D-81279 Munich, Germany*

[d]*Sincrotrone Trieste, Strada Statale S.S. 14, km 163.5, 34012 Basovizza, Trieste, Italy*

Abstract

The Controlled-Drift Detector is a fully-depleted silicon detector that allows 2-D position sensing and energy spectroscopy of X-rays in the range 1-20 keV with excellent time resolution. Its distinctive feature is the simultaneous readout of the charge packets stored in the detector by means of a uniform electrostatic field leading to readout times of few μs. The advantage of this readout mechanism is twofold: i) a higher frame rate/better time resolution with respect to the Charge Coupled Device which represent the reference X-ray spectroscopic imager and ii) a lower contribution of the thermal noise due to a shorter integration time, leading to an excellent energy resolution also at room temperature. In this work we present the first experimental characterization of the Controlled-Drift Detector with synchrotron light in the range 8-30 keV carried out at Sincrotrone Trieste. 2-D energy-resolved radiographic images carried out at a frame frequency up to 100 kHz are shown. Application of the Controlled-Drift Detector to elemental absorption contrast imaging is also presented**.**

Keywords: Controlled drift detector; x-ray spectroscopy ;

1. Introduction

The high brilliance, high monochromaticity and the high collimation degree of synchrotron radiation has pushed the application of synchrotron light in several fields of science and technology [1, 2, 3]. The acceleration in the development of synchrotron light sources and in the associated optical components has not been accompanied by a similar development in the detection systems. Especially detectors with high-count capability as well as excellent time resolution are required in order to exploit these areas and hence the potential of modern synchrotron sources.

* Corresponding author. Tel.: +39 022399 6321; fax: +39 022399 6309; e-mail: Andrea.Castoldi@polimi.it.

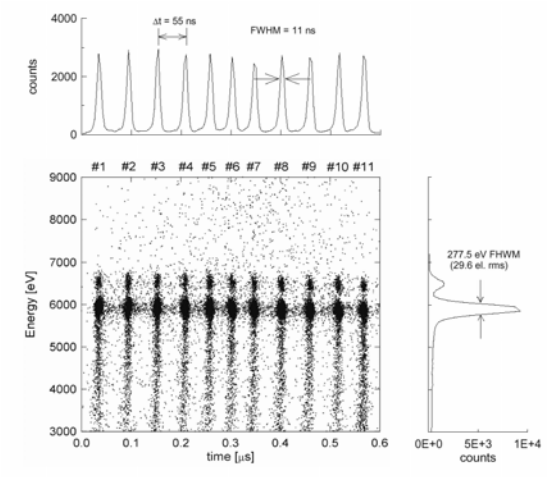

Fig.1.: Scatter plot energy vs drift time of the X-rays of a 55Fe source collected by irradiating a column of the CDD at 100 kHz frame frequency. The integration time was set to 9 μs and the readout time to 1 μs. The upper inset shows the distribution of the events along the time axis. The inset on the right end shows the total distribution of the event energies (i.e. the spectrum of the 55Fe source collected by all the pixels).

In this paper we present the results of the first characterization of the Controlled-Drift Detector, a novel detector for single-photon X-ray imaging carried out at the SYRMEP beamline of Sincrotrone Trieste. The Controlled-Drift Detector is a promising device for high-resolution energy-and time-resolved X-ray radiography. Section 2 is devoted to the description of the Controlled-Drift Detector working principle and achievable performances. Section 3 presents the experimental results obtained at Sincrotrone Trieste.

2. Detector performances

The Controlled-Drift Detector (CDD) [4,5] is a new imaging detector for X-rays in the range 1 - 20 keV. The device is fully depleted and it is operated in integrate – readout mode. The basic idea of the CDD is to generate potential wells in spite of a superposed uniform drift field during the integration mode. In this way the signal electrons are fully confined. During the readout mode a nearly uniform drift field transports the integrated electrons to the readout electrode.

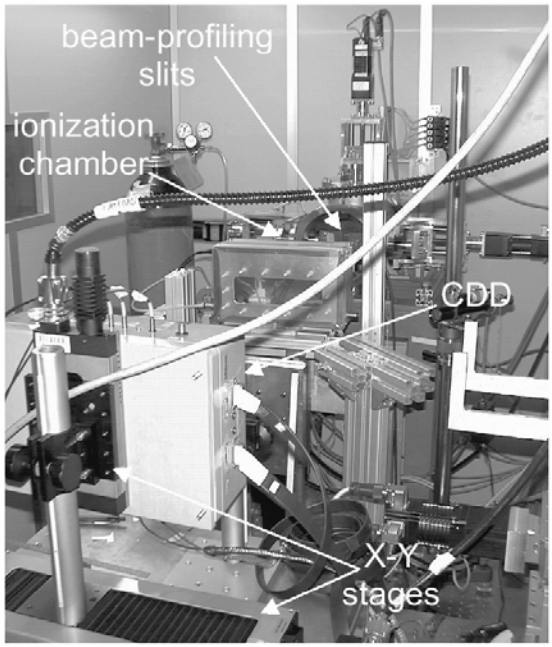

Fig.2.: Photo of the experimental setup at the SYRMEP beamline (Sincrotrone Trieste).

The time between the removal of the barriers and the arrival of the signal electrons to the collecting anodes gives the position of the illuminated "pixel" in the drift direction. The second coordinate is obtained from the granularity of the readout electrodes. The energy of the X-ray is measured by the signal charge with spectroscopic resolution thanks to the low output capacitance and the on-chip front-end electronics. Drift velocities in the range 0.2-0.5 cm/μs have been measured [6] and should lead to readout times of the order of 3-5 μs for a 1 cm-long detector. The fast transport mechanism allows integration times of few tens of μs which is the key to obtain room-temperature energy resolution close to the one obtainable with state-of-the-art X-ray imagers typically operating at cryogenic temperatures and lower frame frequency. Fig. 1 shows the scatter plot energy vs. drift time (i.e. position) of the detected events detected by a single column when the CDD is operated at 100 kHz frame rate. Moving along the time axis we see that the events are gathered in well separated clusters centered at about 6 keV (the Mn K_α and Mn K_β lines can be clearly distinguished) indicating the illuminated pixels.

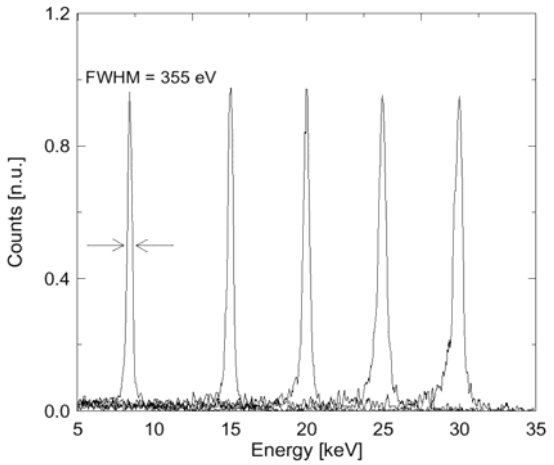

Fig.3.:Normalized-counts energy spectra of several energies in the range 8.5 keV – 30 keV, available at the SYRMEP beamline (Sincrotrone Trieste).

The upper inset of Fig. 1 shows the distribution of the events along the time axis. The FWHM of the peaks is about 20%, leaving a margin for reduction of the pixel size along the drift coordinate (actual size is 180 μm).

The inset on the right end of Fig. 1 shows the total distribution of the event energies (i.e. the spectrum of the ^{55}Fe source collected by all the pixels in the column). The energy resolution at the Mn K_α line (5.899 keV) is 277.5 eV FWHM, corresponding to an Equivalent Noise Charge (ENC) of 29.6 electron r.m.s.

3. X-ray imaging

We have performed several imaging tests in the harsh environment of the SYRMEP beamline at ELETTRA Sincrotrone Trieste (Italy) taking benefit of the highly collimated beam that is available in a synchrotron facility. The experimental setup is shown in Fig. 2.

An ionization chamber was available in front of the detector to monitor the X-ray beam intensity. The CDD was mounted on X-Y stages to pan the detector in order to cover the whole image area. The CDD was always operated at room temperature at frame frequencies in the range 20 kHz – 100 kHz.

a)

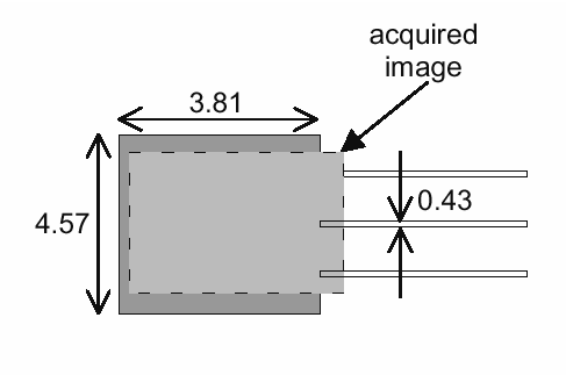

b)

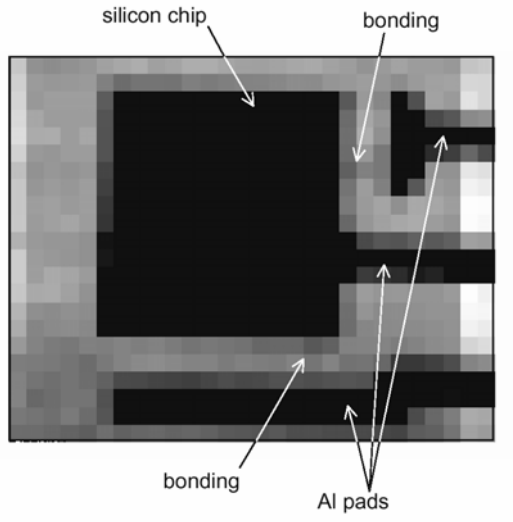

Fig.4: a.) Front view of the radiographed integrated circuit in a TO92 plastic package. b). Radiography of the integrated circuit shown in a). The energy of the X-ray beam was set to 22 keV. The CDD was operated at 100kHz frame rate. The darker the pixel in the gray scale, the lower the number of counts in the pixel. The arrows indicate the bonding connections of the silicon chip to the metal pads.

Fig. 3 shows a scan of the available energies at the SYRMEP beamline in the range 8.5 – 30 keV performed with the CDD operated at 100kHz frame frequency. The achieved energy resolution at 8.5 keV is 355 FWHM, corresponding to an ENC of 38 electron rms.

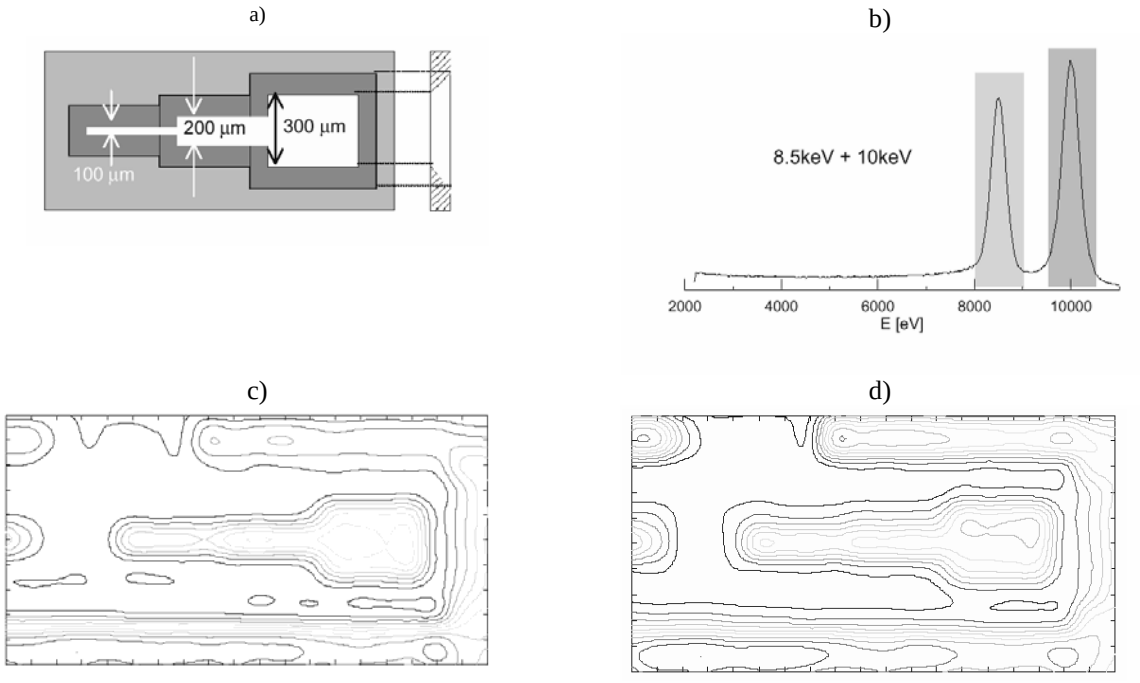

Fig. 5. a) Scheme of principle of the radiographed Silicon slit. b) Energy spectrum acquired by the CDD. The data of the irradiation with a 8.5 keV and the one of the irradiation at 10keV have been summed. The two energy windows used to calculate the images shown in c) and d) are indicated. c) Image of the slit irradiated with 8.5 keV. d) Image of the slit irradiated with 10keV.

The worsening in the resolution is due to external pick-up in the experimental hatch.

3.1. 2-D radiography

The first object that we radiographed is an integrated circuit packaged in a TO92 plastic case. Fig.4a shows a front view of the imaged object. The CDD was operated at 20 kHz frame frequency and the energy of the incident beam was set to 22 keV high enough to pass through the plastic case.

The obtained radiography is shown in Fig. 4b. As shown by the two arrows it is possible to distinguish the bonding connections of the silicon chip to the metal pads.

3.2. Energy resolved radiography

In order to test the energy-discrimination capability of the CDD we performed a radiography of the isotropically etched silicon slit shown in Fig. 5a at two different energies (8.5 keV and 10 keV). The CDD was operated at 100 kHz frame frequency. In order to evaluate the energy-resolved imaging capability of the CDD we joined the data of the two measurements and we processed the data as they were the result of a single measurement performed by two-energy beam. The final energy spectrum is shown in Fig. 5b. By properly windowing the data across the two peaks we obtained the reconstructed contour image at 8.5 keV and 10 keV shown in Fig. 5c and 5d respectively. The less penetrating 8.5 keV X-rays produces an image of smaller extension and with sharper borders compared to 10 keV X-rays.

a)

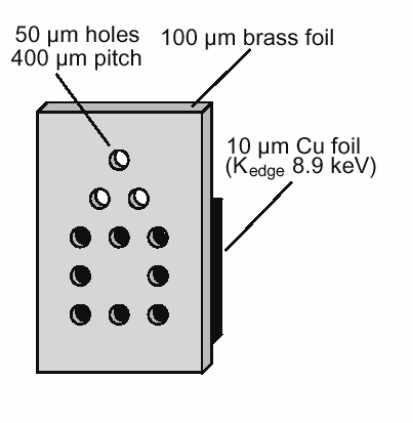

b) c)

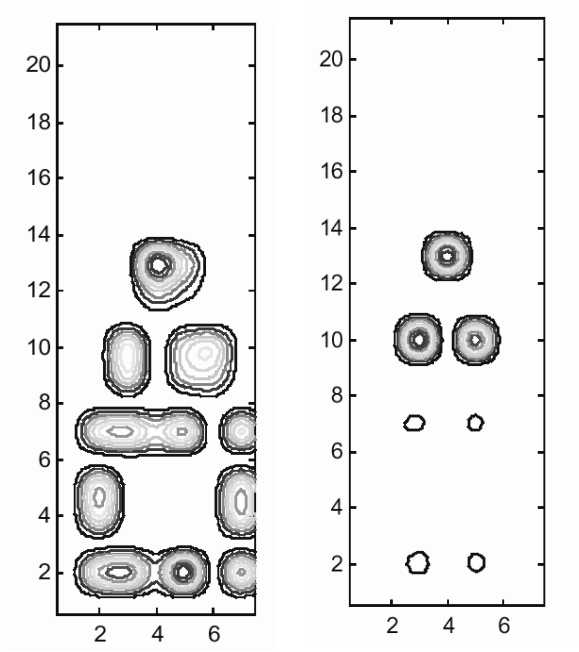

Fig. 6.: a) Scheme of principle of the phantom used to perform elemental absorption contrast imaging. b) Contour plot of the counts recorded by the CDD when the mask was irradiated with 8.5 keV X-rays (below the Cu K-edge). c) Contour plot of the counts recorded by the CDD when the mask was irradiated with 10 keV X-rays (above the Cu K-edge).

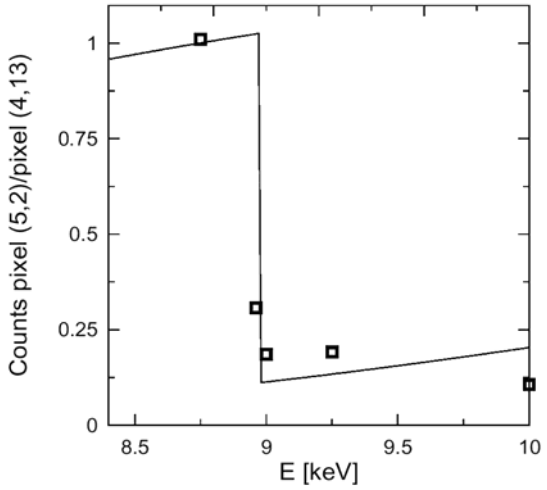

Fig. 7.: Normalized transmittivity of a 10 µm thick Copper layer as a function of the energy around the K-edge. The squares are the experimental points and the line is the theoretical behavior.

The transition between the 200 µm slit and the 100 µm slit is partly hidden due to the pixel size of the present prototype.

This very simple experiment demonstrated the possibility of performing energy-resolved radiography using a polychromatic beam as the one coming from a conventional X-ray generator.

3.3. Elemental absorption contrast imaging

We wanted also to test the performances of the CDD in elemental absorption contrast imaging [7]. With this technique it is possible to image the distribution of known element in a sample by comparing the transmitted image above and below the absorption edge. A drilled mask with some holes blinded by a 10 µm-thick Copper layer (see Fig. 6a) was imaged at different energies of the incident beam below and above the Cu K-edge energy (8.9 keV). Fig. 6b shows the contour plot of the counts recorded at 8.5 keV (below the Cu K-edge), while Fig. 6c shows the one at 10 keV (above the Cu K-edge). At 8.5 keV the transmission of a 10µm-thick Cu layer is nearly one and all the holes are clearly visible showing the shape of a “naif” house. At 10 keV the Cu absorption coefficient increases by a significant

factor and only the triangular roof of the house appears. The difference between these two images will precisely reveal the copper distribution in the sample.

Fig. 7 shows the normalised transmittivity of a 10μm thick Copper layer [8] as a function of the energy across the K-edge (continuous line). The squares are the experimental values obtained by normalising the counts in pixel (5,2) (blinded by the Cu layer) to the ones in pixel (4,13) (passing hole). As it can be noticed the agreement between the experimental points and the theoretical behaviour is very good. Profiting of the energy-resolving capability of the CDD the elemental absorption contrast imaging technique can be performed also with conventional X-ray generators that provide a broad-band spectrum instead of the highly monochromatic light coming out from a synchrotron.

Acknowledgment

The authors gratefully acknowledge S.Masci for the careful bonding of the detector chip and F.Arfelli D. Dreossi and the staff of the SYRMEP beamline for their help during the experimental measurements at the SYRMEP beamline. The authors also wish to thank G.Cerullo for laser drilling the mask used to perform elemental absorption contrast imaging.

References

[1] H.J. Besch, Nucl. Instr. Meth. A419 (1998) 202.
[2] P..Datte et al., Nucl. Instr. Meth. A421 (1999) 576.
[3] S.M. Gruner, Science 238 (1987) 305.
[4] Patents: EP0862226, US 6,249,033.
[5] A.Castoldi, C.Guazzoni, P.Rehak, L.Strüder, IEEE Trans. Nucl. Sci. 48 (2001) 982.
[6] A.Castoldi et al., Nucl. Instrum. Meth. A439 (2000) 519.
[7] Z. H. Levine, B. Ravel, J. Appl. Phys. 85 (1999) 558.
[8] B.L. Henke, E.M. Gullikson, and J.C. Davis, Atomic Data and Nuclear Data Tables 54 (1993) 181.